Frequency-Voltage-var Function for VFD in Oil and Gas Platform with Wind Power

Kassiane de Sousa Medeiros
Graduate Program in Electrical Engineering
Universidade Federal de Minas Gerais
Belo Horizonte, Brazil
kassiane@ufmg.br

João Marcus Soares Callegari
Graduate Program in Electrical Engineering
Universidade Federal de Minas Gerais
Belo Horizonte, Brazil
jmscallegari@ufmg.br

Lorrana Faria da Rocha
Department of Electric Energy
Norwegian University of Science and Technology
Trondheim, Norway
lorrana.faria@ntnu.no

Danilo Iglesias Brandao
Graduate Program in Electrical Engineering
Universidade Federal de Minas Gerais
Belo Horizonte, Brazil
dibrandao@ufmg.br

Abstract—Renewable energy resources emerge as a sustainable alternative to augmenting the energy supply of Floating Production Storage and Offloading (FPSO) platforms. However, the increased generation based on converter-interfaced energy decreases the system-equivalent inertia constant, which becomes more susceptible to frequency deviations. This paper proposes and evaluates the performance of the combined frequency-voltage-var control to mitigate frequency variation in a typical FPSO unit with penetration of wind power systems. The control functions are communication-free and embedded in two active front-end variable frequency drives (AFE-VFDs) set on water injection pumps. The FPSO's electrical power system model is developed in MATLAB/Simulink®. Comparative results with the AFE-VFD equipped with volt-var, freq-var, and combined freq-volt-var functions are shown to highlight the merits of the proposed solution.

Index Terms—Floating production storage and offloading, isolated power system, power quality, volt-var control, freq-var control.

I. INTRODUCTION

The discovery of remote oil fields motivates the employment of Floating Production Storage and Offloading (FPSO) for applications in deep-waters (300–1500 m) and ultra-deep-waters wells (beyond 1500 m) [1]. Moreover, sustainable expansion of power generation on FPSOs is highly desired to support production growth while being environmentally friendly. Floating offshore wind power generation has proven to be a viable solution for such a challenge [2]. Nevertheless, the FPSO is isolated from conventional grid, which configures a weak and susceptible to disturbances power system. The inherent intermittency of wind-based generation can affect power quality issues relating to FPSO frequency and voltage. Also, the increase in FPSO power generation through the inclusion of wind-based energy causes a decrease in the inertia constant (H), when compared to increased generation by adding more synchronous generators (SGs) [3].

Droop regulators employed in wind-based power systems connected to offshore platforms are addressed in [4]–[6].

The authors of [4] proposed a control strategy, which aims to balance the power-sharing between the generation units through modified decentralized droop regulators. The authors of [5] showed the improvement derived from voltage (V/Q) and frequency (f/P) control embedded in wind-based systems for stability in offshore oil and gas installations. The authors of [6] proposed a centralized/decentralized coordinated control strategy, in which active front-end variable frequency drives (AFE-VFDs) are driven to support the FPSO electrical power system. By digitally implementing the volt-var (V/Q) curve embedded in AFE-VFDs, reference [6] shows improvement in FPSO voltage regulation during direct on-line of large motors. On the other hand, at [7] is proposed a frequency-var (f/Q) and voltage-watt (V/P) droop controls, instead of the traditional droop controls (f/P and V/Q), for application in an offshore system with capacitive characteristic connected with a diode-based high voltage direct current (HVDC) link. Herein, the reactive power is processed through the AFE-VFDs installed on the FPSO's largest motors, as in [6].

Strategies for controlling inertia in offshore systems have also have attracted the attention of researchers [8]–[10]. Among the possibilities, synthetic inertia and droop control are widely adopted strategies for frequency support [11]. The droop control is applied in [5], [10], and the synthetic inertia is used in [8], [9]. The authors of [10] propose a strategy that includes primary frequency control based on droop control mechanisms, from offshore wind farms connected through a multi-terminal HVDC network. While the reference [8] proposes tracking-differentiator-based dynamic virtual inertia control, the authors of [9] adopted energy storage systems as a solution to provide virtual inertia emulation. However, solutions that require additional space and weight are quite challenging for offshore applications.

To avoid footprint allocation for new equipment on the FPSO, this paper proposes a decentralized control solution implemented on the VFDs already installed on the FPSO.
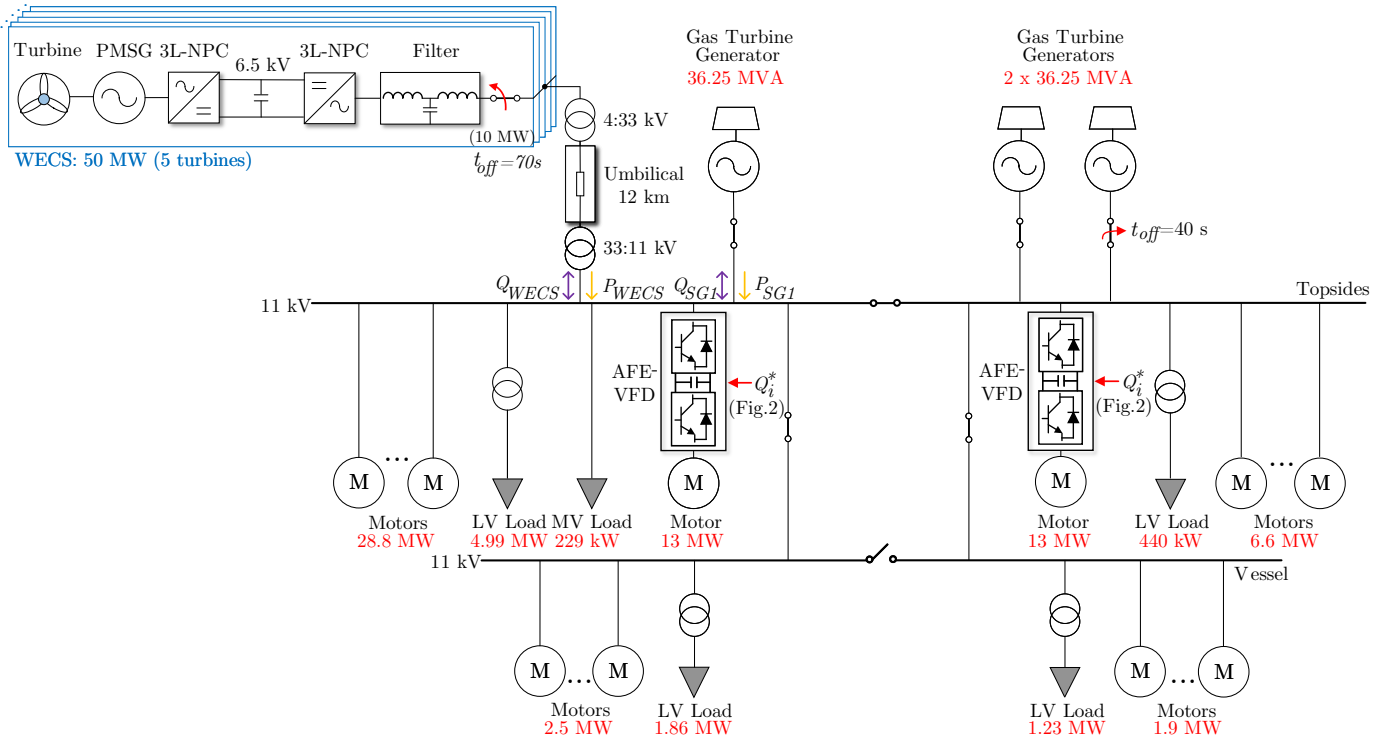
Fig. 1. Simulated electrical power system of a typical Brazilian FPSO from Mero Oil Field with two AFE-VFDs.

The platform's two largest motors are equipped with diode front-end variable frequency drives (DFE-VFDs) to improve efficiency, AC speed control, soft start, and limitation of motor transient short-circuit current contribution. The drawback of their installation is to reduce the equivalent system inertia because they electrically decouple the motors from the main busbar. The insertion of the wind energy conversion system (WECS) also decreases the equivalent FPSO inertia, since this increase in power generation is with a null inertia increment. Hence it is expected to raise voltage and frequency variation on the FPSO, which may beyond the standard limits. In this context, the use of AFE-VFDs embedded with active and reactive functions to regulate voltage and frequency, as well as increasing equivalent inertia is highly desirable.

Thus, this paper proposes and evaluates the performance of the combined frequency-voltage-var (freq-volt-var) function to mitigate frequency variation in FPSO due to the connection of the WECS. The proposed freq-volt-var function takes precedence of frequency over voltage support. The FPSO electrical power system is simulated in MATLAB/Simulink®. The proposed strategy is compared with two other functions found in literature: volt-var and freq-var. The figures of merit used to evaluate the control performance, during steady state conditions and disturbance events, are: voltage and frequency fluctuations, frequency nadir, rate of change of frequency (RoCoF), and inertia constant. Conclusions are based on the improvement of the aforementioned figures of merits during both conditions.

This paper is structured as follows. Section II presents the FPSO electrical power system and the considered figures of merits. Section III shows the features of the frequency and voltage control as functions of the reactive power processed by the AFE-VFDs. Comparative simulation results are shown in Section IV. Finally, Section V presents the conclusions provided by this study.

II. FPSO UNIT WITH FLOATING OFFSHORE WIND

Fig. 1 shows the 50 MW wind farm integrated through the 12 km umbilical cable to the electrical power system of a typical Brazilian FPSO from Mero Oil Field. Herein is employed five WECS, each one composed of a 10 MW wind turbine, with a permanent magnet synchronous generator (PSMG), and a back-to-back converter with an LCL output filter, controlled in grid-following mode to minimize the umbilical cable transmission losses. The FPSO primary power source is composed of three 36.25 MVA SGs driven by 29 MW gas turbines, each one providing an inertia of 1.56 s to the FPSO. The SGs are equipped with frequency and voltage slow dynamic secondary control to achieve steady state regulation at 60 Hz and 11 kV, respectively. Two busbars, Topsides and Vessel, are connected to medium voltage (MV) passive loads, low-voltage (LV) loads fed by step-down transformers, and MV motors (compressors, water injection pumps, etc.). The motors also store kinetic energy in their rotors, which contributes to frequency stability and FPSO inertia. The circuit breakers between the Topsides and Vessel buses are closed as shown in Fig. 1. In this configuration, a radial system is
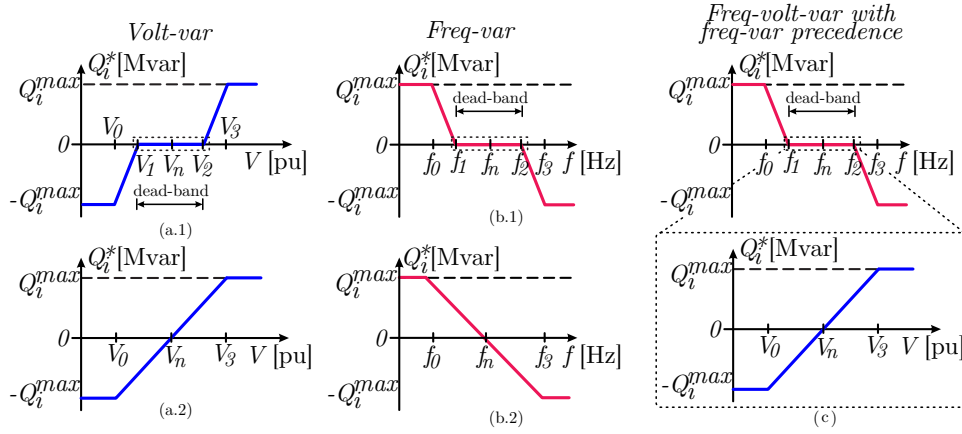
Fig. 2. Communication-free functions digitally implemented on the i-th AFE-VFD: (a.1) volt-var with dead-band; (a.2) volt-var without dead-band; (b.1) freq-var with dead-band; (b.2) freq-var without dead-band; and (c) freq-volt-var with freq-var precedence.

formed, simplifying the protection functions required for the safe operation of the FPSO.

The case study of this paper contains two AFE-VFDs of 16 MVA driving the water injection pumps, as shown in Fig. 1. With the development of power electronics-based technologies, the connection of crucial equipment through VFDs has become a widely accepted solution to mitigate the drawbacks of the all-electric FPSO [12]. Among the commercially available topology, the cascaded H-bridge converter with diode front-end rectifier is a cost-effective solution widely used [13], with reliable speed and torque control of the onboard motors with minimum maintenance requirements. However, the passive rectifier stage produces high levels of harmonic distortion, which is undesirable in offshore systems [14]. This issue is overcome by employing the AFE-VFD, in which the input waveform is less harmonic polluted, feature 4-quadrant speed-torque operation (allowing energy regeneration from the motor to the main feeder) and grid-side unity PF operation [15]. The parameters and details of the models of each equipment adopted are found in [16].

A. Evaluated figures of merit

The power system quality issues caused by WECS insertion and the support provided through AFE-VFDs in the FPSO electrical power system are quantified by the following figures of merit:

1) Voltage variation: $\Delta V = V_{max} - V_{min}$.
2) Frequency variation: $\Delta f = f_{max} - f_{min}$.
3) Frequency nadir: f_{nadir}.
4) RoCoF [17]: $RoCoF_{0.5s} = (f_{0.5} - f_0)/0.5$.
5) Inertia constant [18]: $H = -\Delta P/(2 \cdot RoCoF_{0.5s})$.

The minimum and maximum values of voltage and frequency quantities are evaluated within two predetermined time windows, during the steady state condition. The figures of merit f_{nadir}, RoCoF, and H are computed for transient evaluation. f_{nadir} is defined as the minimum frequency reached after the disturbance, and the RoCoF is the time derivative of the power system frequency (df/dt). For transient evaluation

it is typically estimated by using two frequency measurements within a short period (i.e., 0.5 seconds), immediately following a sudden disturbance [17]. Until that time, which is before the response of most turbine governors to the frequency deviation, the system response depends primarily on the size of the contingency and the inertial response of the system. Lastly, H is estimated by the relation between the amount of generation loss and the system RoCoF immediately after the transient event [18]. These measurements are discussed by comparing the communication-free control functions implemented at the AFE-VFDs, to known: volt-var, freq.-var, and combined freq-volt-var.

III. Voltage Control and Frequency Support Using Reactive Power through the AFE-VFDs

Due to the power electronics embedded in the AFE rectifier cells, the reactive power exchanged with the FPSO can be explored to improve voltage and frequency fluctuations at the main busbar of the FPSO. The use of reactive power configures a degree of freedom in AFE-VFDs, in contrast with the active power, which depends on the motor shaft load. The dq-reference frame control loops implemented at the AFE-VFD are described in [16]. Reactive power references of the grid-side converter are calculated by the autonomous control functions and provided for two AFE-VFDs set on water injection pumps.

Figs. 2 (a)-(c) show the communication-free volt-var, freq-var, and freq-volt-var functions locally implemented at AFE-VFDs. According to Fig. 2, the curves are defined by intervals in which the AFE-VFDs give different instructions regarding reactive power injection (Q). Q_i^* is real-time computed based on the i-th AFE-VFD idle power availability, i.e., $\sqrt{(S_{n,i}^{VFD})^2 - (P_i^{VFD})^2}$, in which $S_{n,i}^{VFD}$ and P_i^{VFD} are the rated apparent power and actual active power processed by the i-th AFE-VFD, respectively. All idle reactive power capacity available in AFE-VFDs is exploited, from $-Q_i^{max}$ to Q_i^{max}.

The dead-band defines the voltage desired interval at which the AFE-VFDs do not exchange reactive power with the power
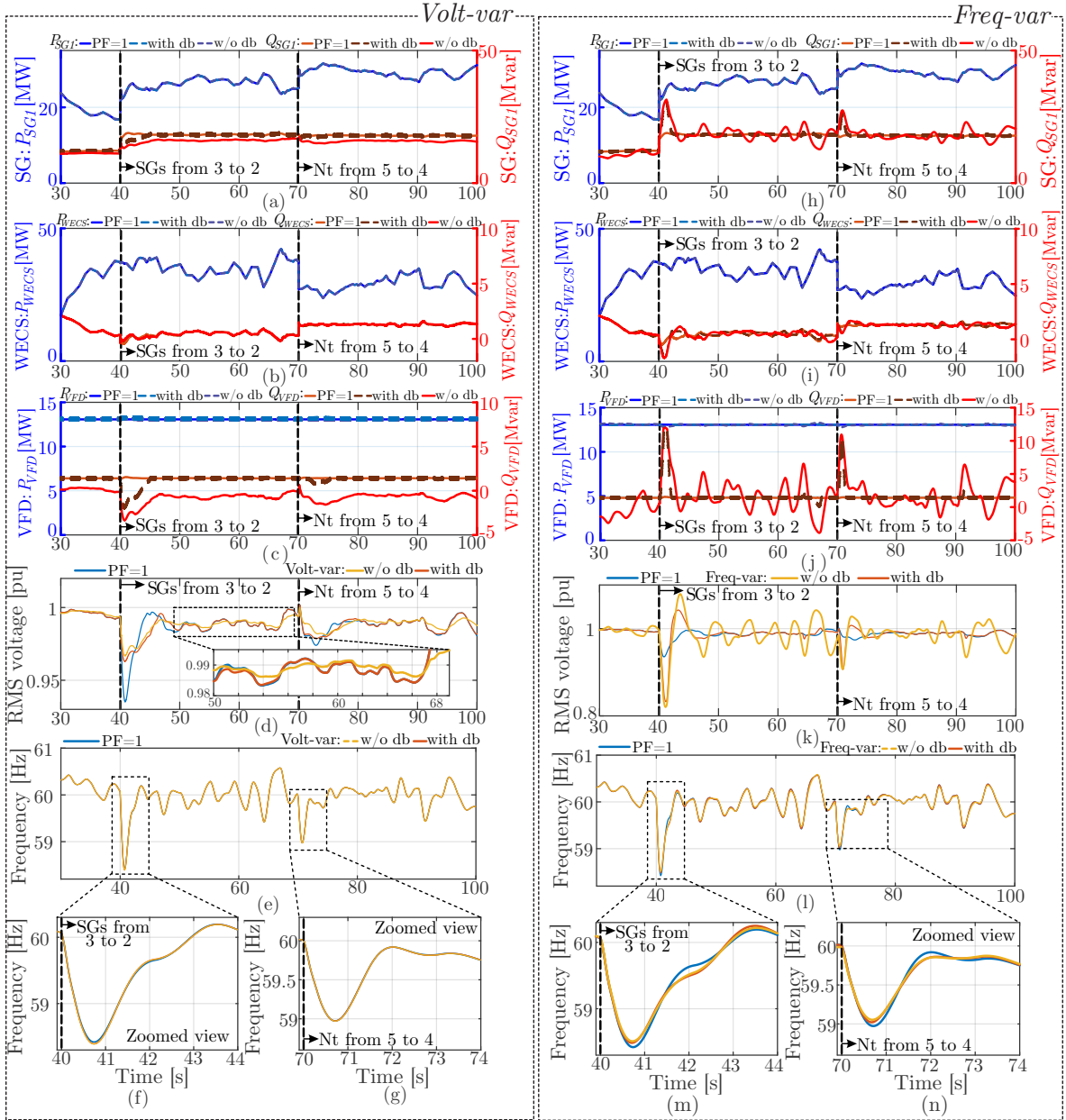
Fig. 3. Volt-var simulated results considering the AFE-VFDs controlled at their output terminals with: unity power factor (PF = 1), volt-var control with dead-band, and volt-var control without dead-band: Active and reactive power at the (a) SG₁, (b) WECS, and (c) AFE-VFD terminals. (d) Main node pu voltage. (e) Measured frequency. (f)-(g) Zoomed views of frequency during transient SG and WECS unscheduled loss events, respectively. Freq-var simulated results considering the AFE-VFDs controlled at their output terminals with: unity power factor (PF = 1), freq-var control with dead-band, and freq-var control without dead-band: Active and reactive power at the (h) SG₁, (i) WECS, and (j) AFE-VFD terminals. (k) Main node pu voltage. (l) Measured frequency. (m)-(n) Zoomed views of frequency during transient SG and WECS unscheduled loss events, respectively.

system. Fig. 2 (a.1) shows the volt-var function with the dead-band defined within V_1 and V_2. For FPSO voltage higher than V_3 or less than V_0, the AFE-VFD processes Q_i^{max} (inductive) and $-Q_i^{max}$ (capacitive), respectively. The volt-var curve is centered on the FPSO-rated voltage, i.e., $V_n = 1$ pu. Similarly, for freq-var function, the dead-band limits are defined within f_1 and f_2, as shown in Fig. 2 (b.1). For FPSO frequency higher than f_3 or less than f_0, the AFE-VFD processes $-Q_i^{max}$ (capacitive) and Q_i^{max} (inductive), respectively. The midpoint

relative to the frequency axis is set to $f_n = 60$ Hz. Figs. 2 (a.2) and (b.2) show the volt-var and freq-var curves without dead-band, while Fig. 2 (c) shows the proposed freq-volt-var curve with frequency support precedence.

A. Volt-var Function

The volt-var function is a well-established piecewise linear curve of voltage as a function of reactive power [19]. This curve can be implemented with or without dead-band, as shown in Figs. 2 (a.1) and (a.2), respectively. The volt-var
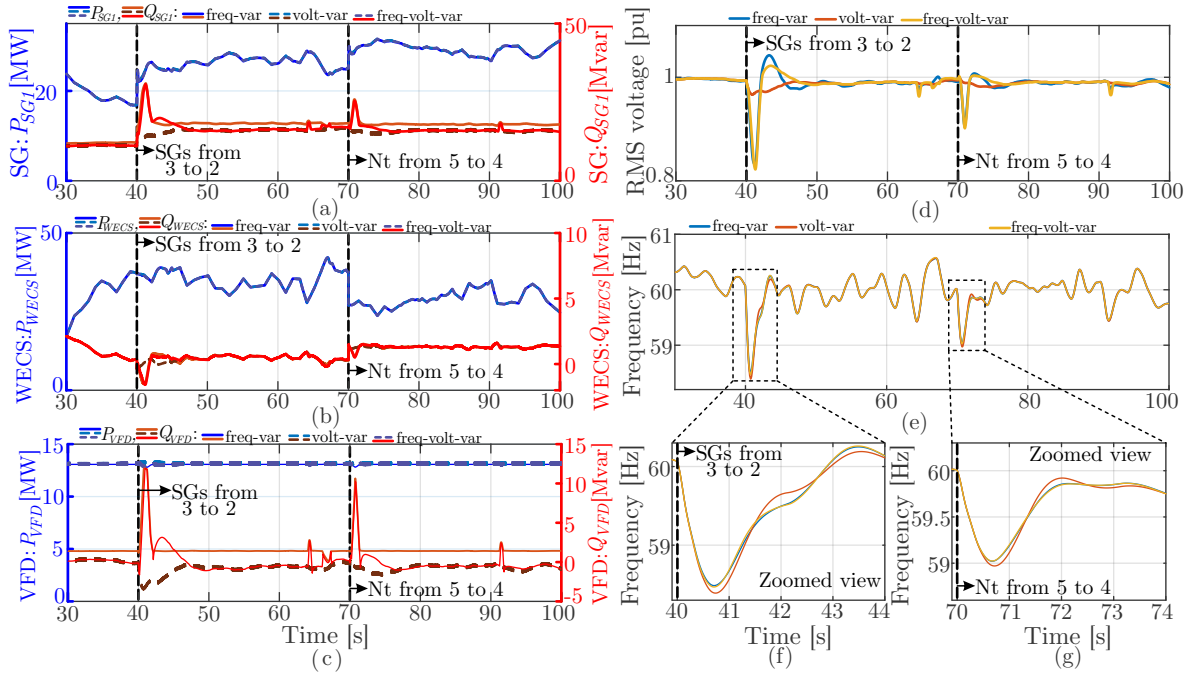
Fig. 4. Simulated results considering the volt-var, freq-var, and freq-volt-var functions implemented in AFE-VFDs: Active and reactive power at the (a) SG$_1$, (b) WECS, and (c) AFE-VFD terminals. (d) Main node pu voltage. (e) Measured frequency. (f)-(g) Zoomed views of frequency during transient SG and WECS unscheduled loss events, respectively.

function with dead-band is described by (1), while the volt-var function without dead-band is described by (2).

$$
Q_i^* = \begin{cases}
-Q_i^{max}, & \text{if } V < V_0 \\
\frac{Q_i^{max}(V-V_1)}{(V_1-V_0)}, & \text{if } V_0 \leq V < V_1 \\
0, & \text{if } V_1 \leq V < V_2 \\
\frac{Q_i^{max}(V-V_2)}{(V_3-V_2)}, & \text{if } V_2 \leq V < V_3 \\
Q_i^{max}, & \text{se } V \geq V_3
\end{cases} \quad (1)
$$

$$
Q_i^* = \begin{cases}
-Q_i^{max}, & \text{if } V < V_0 \\
\frac{Q_i^{max}(2V-V_0-V_3)}{(V_3-V_0)}, & \text{if } V_0 \leq V < V_3 \\
Q_i^{max}, & \text{if } V \geq V_3
\end{cases} \quad (2)
$$

where Q_i^* is the reactive power reference applied to the AFE-VFD control loop [16]. V is the RMS voltage measured at the AFE-VFD output terminals, while $V_0 = 0.95$ pu, $V_1 = 0.925$ pu, $V_2 = 0.975$ pu and $V_3 = 1.05$ are notable points on the curves, defined from the nominal voltage. V_0 and V_3 limit the voltage tolerance of $\pm 5.0\%$, in agreement with standard IEEE 1566 that establishes $\pm 10\%$ as steady-state. V_1 and V_2 bound the dead-band defined herein as $\pm 2.5\%$, half of the tolerance range.

B. Freq-var Function

The freq-var function is defined in Figs. 2 (b.1) and (b.2) with and without dead-band, respectively. It is a piecewise linear curve of frequency as a function of reactive power. The curves with and without dead-band are defined in equations (3) and (4), respectively;

$$
Q_i^* = \begin{cases}
Q_i^{max}, & \text{if } f < f_0 \\
\frac{Q_i^{max}(f-f_1)}{(f_0-f_1)}, & \text{if } f_0 \leq f < f_1 \\
0, & \text{if } f_1 \leq f < f_2 \\
\frac{Q_i^{max}(f-f_2)}{(f_2-f_3)}, & \text{if } f_2 \leq f < f_3 \\
-Q_i^{max}, & \text{if } f \geq f_3
\end{cases} \quad (3)
$$

$$
Q_i^* = \begin{cases}
Q_i^{max}, & \text{if } f < f_0 \\
\frac{Q_i^{max}(2f-f_0-f_3)}{(f_0-f_3)}, & \text{if } f_0 \leq f < f_3 \\
-Q_i^{max}, & \text{if } f \geq f_3
\end{cases} \quad (4)
$$

where f is the frequency estimated by a phase-locked loop (PLL) algorithm from the voltage measurement at the AFE-VFD output terminals. $f_0 = 59$ Hz, $f_1 = 59.5$ Hz, $f_2 = 60.5$ Hz, and $f_3 = 61$ Hz are notable points on the curves, defined from the nominal frequency. f_0 and f_3 limit the frequency tolerance of $\pm 1.67\%$, in agreement with the standard IEC 61892 that set $\pm 5\%$ as steady-state frequency tolerance. f_1 and f_2 bound the dead-band defined herein as $\pm 0.83\%$, half of the tolerance range.

C. Proposed Combined Frequency-Voltage-var Function

The combined freq-volt-var function is shown in Fig. 2 (c). The proposed curve is composed of the volt-var function without dead-band and the freq-var function with dead-band, where the freq-var function precedes the volt-var function i.e.,

frequency deviations greater than f_2 or less than f_1 enable the freq-var curve, as shown in following Eqs. 5 and 6.

$$Q_i^* = \begin{cases} Q_i^{max}, & \text{if } f < f_0 \\ \frac{Q_i^{max}(f-f_1)}{(f_0-f_1)}, & \text{if } f_0 \leq f < f_1 \\ Q_{i\,volt-var}^*, (Eq.\ 6), & \text{if } f_1 \leq f < f_2 \\ \frac{Q_i^{max}(f-f_2)}{(f_2-f_3)}, & \text{if } f_2 \leq f < f_3 \\ -Q_i^{max}, & \text{if } f \geq f_3 \end{cases} \quad (5)$$

$$Q_{i\,volt-var}^* = \begin{cases} -Q_i^{max}, & \text{if } V < V_0 \\ \frac{Q_i^{max}(2V-V_0-V_3)}{(V_3-V_0)}, & \text{if } V_0 \leq V < V_3 \\ Q_i^{max}, & \text{if } V \geq V_3 \end{cases}$$
$$(6)$$

Herein, the notable points (f_0, f_1, f_2, f_3, V_0, and V_3) are: $f_0 = 59$ Hz, $f_1 = 59.5$ Hz, $f_2 = 60.5$, $f_3 = 61$ Hz, $V_0 = 0.95$ pu, and $V_3 = 1.05$ pu.

The proposed freq-volt-var strategy differs from others in literature since the volt-var is triggered in a steady state condition, while the freq-var is triggered under transient events. The proposed control is locally managed based on the AFE-VFDs-driven load demand, therefore active power processing is not considered in the proposed control.

IV. SIMULATION RESULTS

Section IV-A shows a comparison between AFE-VFDs programmed to unity power factor (PF = 1); volt-var with dead-band; and volt-var without dead-band. Section IV-B also addressed three scenarios: AFE-VFDs with PF = 1, freq-var with dead-band, and freq-var without dead-band. The better performances related to the presence or absence of dead-band at the curve are applied to compose combined freq-volt-var control. Section IV-C discusses the combined freq-volt-var from its comparison with volt-var and freq-var. For analysis purposes, this section also presents the figures of merit results for the FPSO without VFDs for the water injection pumps drive (i.e., the 13 MW motors are directly connected to the 11 kV bus), and operating with PF = 1.

The steady state figures of merit (ΔV and Δf) are calculated for time windows of $30 \leq t < 40$ s, $50 \leq t < 70$ s, and $80 \leq t < 90$ s. The following sequence of generation loss is simulated:

- At $t = 40$ s, an unscheduled interruption of one SG is performed ($N_{SG} = 3 \rightarrow 2$);
- at $t = 70$ s, an unscheduled shutdown of one wind turbine is simulated ($N_t = 5 \rightarrow 4$).

Transient events are computed for time windows: $40 \leq t < 44$ s and $70 \leq t < 74$ s.

A. Comparison between PF = 1, volt-var control with dead-band, and volt-var control without dead-band

Figs. 3 (a)-(g) show steady state and transient results for the scenario characterized by AFE-VFDs embedded into the FPSO operating with PF = 1; and equipped with the volt-var curves with and without dead-band. Figs. 3 (a)-(c) show the SG_1, WECS, and AFE-VFDs active and reactive powers, respectively. Due to the power system symmetry and the power-sharing derived from the droop-based control of the SGs, only SG_1 data are addressed. The SGs complement the intermittent active power generated by the WECS, which leads to a natural oscillation in the FPSO frequency as a result of the governor's slow dynamics. Due to the power coupling caused by the FPSO line impedances and to slow dynamics of the SG automatic voltage regulator (AVR), the main busbar voltage also oscillates with the WECS penetration.

From Fig. 3 (c) the reactive power processed by the AFE-VFDs using the volt-var function with dead-band corresponds to the same reactive power curve for PF = 1, except for the seconds that follow the transient events (i.e. loss of SG in 40 s or WECS in 70s). From Fig. 3 (d), after 40 s, the FPSO voltage sag reaches 0.93 pu, considering the AFE-VFDs controlled for PF = 1. On the other hand, the voltage value for volt-var with dead-band improves from 0.93 to 0.96 pu. The most attenuated voltage sag during unscheduled SG outage RMS voltage of 0.97 pu is associated with the implementation of the volt-var control without dead-band. This fact is explained due to a higher positive slope of the volt-var curve with dead-band, in the intervals between V_0 - V_1, and V_2 - V_3 - see Fig. 2 (a.1), compared to the volt-var curve slope without dead-band, between V_0 - V_3 - see Fig. 2 (a.2).

Moreover, during the 50 s to 68 s, steady-state improvement of FPSO voltage regulation is seen when the AFE-VFDs operate with the volt-var curve without dead-band ($\Delta V = 6.94$ x 10^{-3} V) compared to the case with dead-band ($\Delta V = 14.44$ x 10^{-3} V) - see the enlarged view of Fig. 3 (d). On the other hand, no improvement or deterioration is observed in the frequency variation with the presence or absence of the dead-band, during steady-state (i.e., Fig. 3 (c)) or transient (i.e., Figs. 3 (f)-(g)). Due to this lower voltage variation in steady state, the volt-var without dead-band is adopted for the proposed combined freq-volt-var strategy.

B. Comparison PF = 1, freq-var control with dead-band, and freq-var control without dead-band

Figs. 3 (h)-(n) show steady state and transient results for the scenario characterized by AFE-VFDs embedded into the FPSO operating with PF = 1; and equipped with the freq-var curves with and without dead-band. Figs. 3 (h)-(j) show the SG_1, WECS, and AFE-VFDs active and reactive powers, respectively. The reactive power flow control with the freq-var function without dead-band turns the AFE-VFD reactive power profile more oscillatory compared to the case with the volt-var function case. For the volt-var function, the maximum Q_{VFD} injected is 3.35 Mvar in the transient event (after 40 s), and 1.47 Mvar in steady state - see Fig. 3 (c). While for the control function associated with frequency variation, the maximum Q_{VFD} absorbed is 11.97 Mvar in the transient event (after 40 s), and 6.55 Mvar in steady state - see Fig. 3 (j). This more oscillatory reactive power flow affects the FPSO voltage, which is more disturbed with the freq-var function than considering the AFE-VFDs controlled at their output terminals with PF = 1. This voltage behavior is due to the coupling between reactive power flow and voltage,

TABLE I
SUMMARY OF THE RESULTS SAMPLED FROM FIG. 4.

Function Control	Steady-state				Transient-state					
	$30 \leq t < 40s$		$80 \leq t < 90s$		$40 \leq t < 44s$			$70 \leq t < 74s$		
	$N_{SG} = 3, N_t = 5$		$N_{SG} = 2, N_t = 4$		$N_{SG} = 3 \to 2, N_t = 5$			$N_{SG} = 2, N_t = 5 \to 4$		
	ΔV	Δf	ΔV	Δf	f_{nadir}	$ROCOF_{0.5s}$	H	f_{nadir}	$ROCOF_{0.5s}$	H
	(pu)	(Hz)	(pu)	(Hz)	(Hz)	$(1/s^2)$	(s)	(Hz)	$(1/s^2)$	(s)
without AFE-VFDs	7.05×10^{-3}	0.52	5.59×10^{-3}	0.44	58.64	2.55	3.53	59.11	1.61	3.36
PF = 1	6.58×10^{-3}	0.54	4.82×10^{-3}	0.53	58.42	2.92	3.08	58.97	1.87	2.90
volt-var	4.51×10^{-3}	0.54	2.72×10^{-3}	0.53	58.39	2.98	3.02	58.97	1.87	2.91
freq-var	6.58×10^{-3}	0.54	6.59×10^{-3}	0.53	58.49	2.87	3.14	59.02	1.83	2.97
freq-volt-var	4.51×10^{-3}	0.54	2.27×10^{-3}	0.53	58.47	2.90	3.10	59.02	1.82	2.98

which occurs in inductive grids such as the FPSO power system. The largest voltage oscillations are associated with the implementation of freq-var without dead-band. In such a scenario, the voltage variation reaches $\Delta V = 0.26$ pu in the transient event (after the SG shutdown at 40 s) and $\Delta V = 0.11$ pu in steady state condition. The RMS voltage considering the implementation of freq-var with dead-band corresponds to the RMS voltage for PF = 1, except at the instants following the transient events. The voltage variation with freq-var control with dead-band is $\Delta V = 0.03$ pu in the transient event (after the SG shutdown at 40 s) and $\Delta V = 0.01$ pu in steady state.

The frequency behavior during the steady state shows a negligible difference with PF = 1 or with the employment of the freq-var curves - see Fig. 3 (l). On the other hand, after transient events (t = 40 s), the frequency nadir shows a recovery, from 58.42 Hz (PF = 1) to 58.49 Hz (freq-var with dead-band), and 58.51 Hz (freq-var without dead-band) - see Fig. 3 (m). In the second transient (t = 70 s), the following metrics are computed: f_{nadir} = 58.97 Hz (PF = 1), f_{nadir} = 59.02 Hz (freq-var with dead-band), and f_{nadir} = 59.05 Hz (freq-var without dead-band) - see Fig. 3 (n). Given the proximity of frequency nadir between freq-var scenarios with dead-band and without dead-band and the reduced effect on FPSO voltage when employing the freq-var with the dead-band, the proposed combined freq-volt-var strategy employs the dead-band freq-var curve. Thus, it is possible to provide frequency support in transient periods and during steady state do not activate the frequency support.

C. Comparison between volt-var, freq-var, and combined freq-volt-var function

Fig. 4 shows the steady-state and the transient results considering the AFE-VFDs equipped volt-var without dead-band, freq-var with dead-band, and combined freq-volt-var control, considering the function described in Figs. 2 (a.2), (b.1), and (c), respectively. The active and reactive power terms at the SG_1, WECS, and AFE-VFDs terminals are shown in Figs. 4 (a)-(c), respectively. Figs. 4 (d) and (e) show the voltage and frequency profiles, respectively. Tab. I summarizes the figures of merit sampled from Fig. 4. In addition, Tab. I presents the figures of merit for AFE-VFDs controlled with PF = 1 ($Q_i^* = 0$) and for the operation of the FPSO electrical power system without AFE-VFDs.

From Tab. I the FPSO system without VFDs presents the smallest frequency variations in steady-state (0.52 Hz and 0.44 Hz), the highest f_{nadir} values (58.64 Hz and 59.11 Hz) and lowest $|RoCoF|$ values. These enhanced frequency parameters are assigned to the inertia contribution when the two 13 MW water injection pump motors are directly coupled to the main busbar. On the other hand, without AFE-VFDs the AVR control represents the only voltage control of the entire power system. The reactive power absorption by the directly coupled motor to the FPSO main bus deteriorates voltage-related figure of merit compared to the cases with VFD-interfaced motors, resulting in the highest voltage variations, 7.05×10^{-3} pu and 5.59×10^{-3} pu). Reactive power regulation at the VFD output terminals leads to a voltage regulation improvement compared to the case without VFD.

From second line of Tab. I, i.e, VFDs controlled at their terminals with PF = 1, the system inertia decrease and consequently frequency-linked parameters shows deterioration. The implementation of volt-var control (third line of Tab. I), compared to the PF=1 case, improves voltage variation at the same time that continue to deteriorate frequency parameters. Since with volt-var implemented reactive power absorbed for voltage regulation disturbs the frequency. The opposite relation is evidenced when reactive power is injected for frequency regulation (freq-var implemented), the voltage variation is disturbed while frequency parameters show improvement.

During the steady state intervals, with the incorporation of the volt-var in the freq-var function, i.e. the proposed freq-volt-var, an improvement in voltage variation is observed from 6.58×10^{-3} pu (with freq-var) to 4.51×10^{-3} pu (with freq-volt-var) - see Tab. I. Regarding the transient caused by the unscheduled interruption of one SG, the voltage sag reaches 0.83 pu and 0.82 pu with freq-var and freq-volt-var strategies, respectively - see Fig. 4 (d). Due to the freq-var and freq-volt-var dead-bands practically not being violated, a similar Δf is obtained for all strategies during steady state.

Nonetheless, the frequency profile enhancement is noted compared to the volt-var function, as shown in Figs. 4 (f) and (g). For instance, with the SG shutdown at 40 s, the frequency nadir rises from 58.39 Hz (with volt-var) to 58.49 Hz and 58.47 Hz with the employment of freq-var-based strategies (i.e., freq-var, and freq-volt-var, respectively) $|RoCoF|$ value for the disturbance triggered by the shutdown of one wind turbine also shows an improvement: a reduction from 1.87

Hz/s with volt-var to 1.82 Hz/s with combined freq-volt-var for the 70 - 74 s simulated period. Besides, the system inertia constant, calculated using the disturbance triggered by the shutdown of one wind turbine, increases from 2.91 s with volt-var to 2.98 s with freq-volt-var.

V. Conclusions

This paper proposed and evaluated the communication-free freq-volt-var function embedded in AFE-VFDs for frequency support in offshore FPSO systems with high WECS penetration. The evaluation methodology showed that the frequency support via reactive power flow improves the frequency, but disturbs the FPSO voltage. The incorporation of voltage function to the control guarantees the minimization of these distortions during steady state and maintains the improvements in frequency at transient events. Steady-state simulation results from the combined freq-volt-var method showed a reduction of 31.5% in voltage variation compared to the freq-var function. The figures of merit to the transient event of synchronous generator shutdown, frequency nadir, and inertia constant, enhanced by 0.08 Hz and 2.65%, respectively, compared to the volt-var function.

This means that the improvement in frequency and voltage deviations are achieved with absorption and injection of reactive power by the AFE-VFDs, respectively. This conflicting behavior indicates that it is not possible to improve simultaneously voltage and frequency deviation in FPSO power systems by processing only reactive power.

References

[1] R. Brown, "Fpso: lessons learned," *IEEE Industry Applications Magazine*, vol. 10, no. 2, pp. 18–23, 2004.

[2] P. Glaum, F. Neumann, and T. Brown, "Offshore wind integration in the north sea: The benefits of an offshore grid and floating wind," in *2023 19th International Conference on the European Energy Market (EEM)*, 2023, pp. 1–7.

[3] Q. Yu, Y. Liu, Z. Jiang, L. Li, Y. Zhang, and M. Guo, "Study of offshore wind power penetration rate in gas turbine generator platform power grid," *Energy Reports*, vol. 7, pp. 141–146, 2021, iCPE 2020-The International Conference on Power Engineering.

[4] S. D'Arco, A. Petterteig, R. Pittini, and T. M. Undeland, "Droop regulated vscs for island operation of future offshore systems," in *2011 IEEE Trondheim PowerTech*, 2011, pp. 1–6.

[5] A. R. Årdal, T. Undeland, and K. Sharifabadi, "Voltage and frequency control in offshore wind turbines connected to isolated oil platform power systems," *Energy Procedia*, vol. 24, pp. 229–236, 2012.

[6] J. M. S. Callegari, L. A. Vitoi, and D. I. Brandao, "Vfd-based coordinated multi-stage centralized/decentralized control to support offshore electrical power systems," *IEEE Transactions on Smart Grid*, pp. 1–1, 2022.

[7] R. Blasco-Gimenez, S. Añó-Villalba, J. Rodríguez-D'Derlée, F. Morant, and S. Bernal-Perez, "Distributed voltage and frequency control of offshore wind farms connected with a diode-based hvdc link," *IEEE Transactions on Power Electronics*, vol. 25, no. 12, pp. 3095–3105, 2010.

[8] X. Qi, R. Madonski, C. Huang, and Y. Ke, "Tracking-differentiator-based dynamic virtual inertial control of offshore wind power plant for frequency regulation," *International Journal of Electrical Power and Energy Systems*, vol. 141, p. 108150, 2022.

[9] A. A. Adeyemo and E. Tedeschi, "Sizing of energy storage for virtual inertia emulation and primary frequency control in low-inertia systems," in *2022 5th International Conference on Power and Energy Applications (ICPEA)*, 2022, pp. 480–486.

[10] B. Silva, C. L. Moreira, L. Seca, Y. Phulpin, and J. A. Pecas Lopes, "Provision of inertial and primary frequency control services using offshore multiterminal hvdc networks," *IEEE Transactions on Sustainable Energy*, vol. 3, no. 4, pp. 800–808, 2012.

[11] Y. Cheng, R. Azizipanah-Abarghooee, S. Azizi, L. Ding, and V. Terzija, "Smart frequency control in low inertia energy systems based on frequency response techniques: A review," *Applied Energy*, vol. 279, p. 115798, 2020.

[12] C.-L. Su, W.-L. Chung, and K.-T. Yu, "An energy-savings evaluation method for variable-frequency-drive applications on ship central cooling systems," *IEEE Transactions on Industry Applications*, vol. 50, no. 2, pp. 1286–1294, 2014.

[13] N. Zargari, Z. Cheng, and R. Paes, "A guide to matching medium voltage drive topology to petrochemical applications," in *2017 Petroleum and Chemical Industry Technical Conference (PCIC)*, 2017, pp. 133–142.

[14] W. Liu, T. Tarasiuk, C.-L. Su, M. Gorniak, M. Savaghebi, J. C. Vasquez, and J. M. Guerrero, "An evaluation method for voltage dips in a shipboard microgrid under quasi-balanced and unbalanced voltage conditions," *IEEE Transactions on Industrial Electronics*, vol. 66, no. 10, pp. 7683–7693, 2019.

[15] Z. Yang, J. Sun, Y. Tang, M. Huang, and X. Zha, "An integrated dual voltage loop control for capacitance reduction in chb-based regenerative motor drive systems," *IEEE Transactions on Industrial Electronics*, vol. 66, no. 5, pp. 3369–3379, 2019.

[16] H. M. A. Antunes, D. I. Brandao, V. H. M. Biajo, M. H. S. Alves, F. S. Oliveira, and S. M. Silva, "Floating, production, storage, and offloading unit: A case study using variable frequency drives," in *IEEE IAS Annual Meeting*, 2022, pp. 1–6.

[17] NERC, "Fast frequency response concepts and bulk power system reliability need: Nerc inverter-based resource performance task force," *North American Electric Reliability Corporation*, pp. 1–29, 2020.

[18] T. Inoue, H. Taniguchi, Y. Ikeguchi, and K. Yoshida, "Estimation of power system inertia constant and capacity of spinning-reserve support generators using measured frequency transients," *IEEE Transactions on Power Systems*, pp. 136–143, 1997.

[19] I. S. 1547-2018, "Ieee standard for interconnection and interoperability of distributed energy resources with associated electric power systems interfaces," *(Revision of IEEE Std 1547-2003)*, vol. 261, pp. 1–138, 2018.